CDDpress

www.nature.com/cdd

ARTICLE

Check for updates

PPA1 promotes adipogenesis by regulating the stability of C/EBPs

Yangyang Wu[1,2,4], Yue Sun[3,4], Yuqing Song[1], Jiateng Wang[1], Ye Han[1], Nan Yang[1], Haiyan Lin[1✉], Ye Yin[1✉] and Xiao Han[1✉]

Adipogenesis significantly contributes to healthy adipose tissue expansion in obesity. Increasing adipocyte number or function to alleviate adipose tissue overload could serve as a therapeutic strategy for both lipodystrophy and obesity-related metabolic syndrome. Inorganic pyrophosphatase (PPA1) is an enzyme that catalyzes the hydrolysis of pyrophosphate (PPi) and is involved in many biochemical reactions, but its function in adipose tissue has not been studied previously. In this study, we demonstrated that adipose-specific PPA1 knockout ($PPA1^{AKO}$) mice showed lipodystrophy and spontaneously developed hepatic steatosis and severe insulin resistance under normal chow diet feeding. PPA1 deficiency suppressed the differentiation of primary adipocyte precursors and 3T3-L1 cells. Notably, PPA1 overexpression can restore inhibited adipogenesis in preadipocytes isolated from *db/db* mice and type 2 diabetes patients. Mechanistic studies have revealed that PPA1 acts as a positive regulator of early adipocyte differentiation by promoting CCAAT/enhancer-binding proteinβ and δ (C/EBPβ and δ) protein stability. Moreover, the function of PPA1 in adipogenesis is independent of its PPi catalytic activity. Collectively, our in vivo and in vitro findings demonstrated that PPA1 is a novel critical upstream regulator of adipogenesis, controlling adipose tissue development and whole-body metabolic homeostasis.

Cell Death & Differentiation; https://doi.org/10.1038/s41418-024-01309-2

INTRODUCTION

Adipose tissue plays a critical role in regulating energy balance and nutrient homeostasis. Its expansion occurs through adipocyte hyperplasia (an increase in cell number), hypertrophy (an increase in cell size), or both [1]. Studies reveal that white adipose tissue (WAT) from patients with metabolic disorders often exhibits hypertrophic adipocytes and proinflammatory macrophages [2, 3]. Conversely, metabolically healthy obesity is characterized by adequate WAT expansion, primarily through adipocyte hyperplasia and limited ectopic lipid deposition [4, 5]. Recent studies suggest that the capacity to recruit new fat cells through adipogenesis is a key determinant of healthy adipose tissue expansion during overfeeding, and increased adipogenesis can protect other tissues from Triglyceride (TG) accumulation, insulin resistance, and metabolic dysfunction [6]. Adipogenesis is a two-step process in which the fibroblast-like progenitor cells transform into triglyceride-filled mature adipocytes. In the first step (also called the commitment step), the fibroblast-like cell restricts itself to form a preadipocyte. Subsequently, during differentiation, preadipocytes undergo growth arrest and eventually form functional, insulin-responsive mature adipocytes [7]. Impaired adipogenesis resulting from heterogeneous genetic or acquired causes can lead to lipodystrophy, characterized by generalized or partial loss of adipose tissue [8]. Given that adipose tissue plays a crucial role in regulating energy balance and systemic metabolic homeostasis, adipocyte loss often leads to metabolic complications, such as insulin resistance, diabetes, and nonalcoholic fatty liver disease [9, 10].

Over the past decades, significant progress has been made in understanding the transcriptional control mechanisms involved in adipocyte differentiation [11]. The central role of PPARγ in adipogenesis has been supported by overwhelming evidence from studies both in vivo and in vitro. Although the physiological ligand of PPARγ in adipose tissue is still unknown, synthetic thiazolidinedione drugs (TZDs) are used as potent PPARγ ligands for the treatment of diabetes by stimulating adipogenesis. Patients treated with TZDs often experience weight gain, which is associated with WAT hyperplasic expansion. This healthy remodeling of adipose tissue in patients treated with TZDs often appears metabolically favorable and contributes to systemic insulin sensitivity [6, 12, 13].

A majority of identified activators or suppressors of adipogenesis have been found to directly or indirectly modulate PPARγ expression or transcription activity. Among these regulators are CCAAT/enhancer-binding proteins (C/EBPs), a group of basic leucine zipper family transcription factors (TFs) that are crucial for adipocyte differentiation [14]. During hormonal treatment-induced adipocyte differentiation in vitro, it is well-established that isobutylmethylxanthine (MIX) and dexamethasone (DEX) can induce expression of C/EBPβ and C/EBPδ, respectively, in the very early stages of adipogenesis. These two TFs then collaborate to up-regulate the expressions of PPARγ and C/EBPα [15, 16]. Studies in 3T3-L1 and NIH-3T3 cell lines have confirmed that inhibition of either C/EBPs results in attenuated adipogenesis [17]. Moreover, in vivo studies have revealed that deletion of C/EBPβ and C/EBPδ

[1]Key Laboratory of Human Functional Genomics of Jiangsu Province, Department of Biochemistry and Molecular Biology, Nanjing Medical University, Nanjing, Jiangsu, China. [2]Women's Hospital of Nanjing Medical University, Nanjing Women and Children's Healthcare Hospital, Nanjing Medical University, Nanjing, China. [3]Department of Cardiology, Nanjing First Hospital, Nanjing Medical University, Nanjing, China. [4]These authors contributed equally: Yangyang Wu, Yue Sun. ✉email: linda@njmu.edu.cn; yin@njmu.edu.cn; hanxiao@njmu.edu.cn

Received: 3 August 2023 Revised: 24 April 2024 Accepted: 1 May 2024
Published online: 18 May 2024

leads to defective adipose tissue development in mice [18]. In addition to playing an important role in the activation of C/EBPα and PPARγ, C/EBPβ has been reported to have other functions during adipocyte differentiation, such as regulating mitotic clonal expansion (MCE) and modulating autophagy [19, 20]. As important TFs in adipocyte differentiation, C/EBPs can be regulated not only by transcription but also by translational and post-translational modifications (PTM) [7].

PPA1 is an enzyme responsible for catalyzing the hydrolysis of pyrophosphate to inorganic phosphate, a highly exergonic reaction that can be coupled to some energy-demanding biochemical reactions. This enzyme is suggested to play a critical role in various biosynthetic reactions, including bone formation, collagen synthesis, DNA synthesis, and neurite growth [21, 22]. A series of studies on PPA1 in mammals have reported high expression levels of PPA1 in various cancer cells, such as breast cancer, colorectal cancer, hepatocellular carcinoma, and ovarian cancer [23–26]. Further study has suggested that PPA1 can promote cell proliferation and inhibit cell apoptosis, depending on TP53 expression and JNK activation, with its pyrophosphatase activity being essential for PPA1-mediated cell proliferation [23]. Beyond its role in cancer cells, studies have also reported that PPA1 regulates neurite growth via JNK dephosphorylation in mouse neuroblastoma cells, induces type I collagen synthesis, and stimulates calcification by osteoblasts [21, 22]. However, the role of PPA1 in metabolic syndromes has not been studied. A previous study in our lab has reported that global heterozygous PPA1$^{+/-}$ mice developed insulin resistance and metabolic impairments under high-fat-diet feeding. Despite increased lipid accumulation in non-adipose tissues in PPA1$^{+/-}$ mice, the reduction in adipose tissue weight has drawn our interest, as the adipose tissue is typically the principal tissue for excess energy storage [27].

Therefore, in this study, we generated adipose-specific PPA1 knockout (PPA1^{AKO}) mice and investigated the role of PPA1 in adipose tissue in vivo. Deletion of PPA1 resulted in lipodystrophy affecting both white and brown adipose tissues (BAT), leading to metabolic disorders. Further in vitro studies revealed that the loss of PPA1 may inhibit the PPARγ signaling pathway by promoting C/EBPβ and C/EBPδ degradation, which subsequently attenuates adipogenesis. More importantly, the pyrophosphatase activity of PPA1 is not required for its regulation of adipogenesis. Taken together, our data suggest that PPA1 functions as an important upstream regulator of adipocyte differentiation in an enzymatic-independent manner, and targeting PPA1 may represent a novel therapeutic approach for metabolic disorders.

RESULTS

PPA1 ablation results in severe lipodystrophy in vivo

To evaluate the specific role of PPA1 in adipose tissue, adipose-specific PPA1-knockout (PPA1^{AKO}) mice were generated, as shown in Fig. S1A. PPA1 was specifically deleted in BAT and WAT, respectively, but not in any other tissues detected (Fig. S1B). Then, the mice were fed with a normal chow diet (NCD). The PPA1^{AKO} mice were morphologically indistinguishable from their wild-type (WT) littermates (Fig. 1A). Although no differences in body weight were observed, analysis of epididymal WAT (eWAT) and inguinal WAT (iWAT) revealed significant decreases in both fat pads, a similar result to that observed in BAT (Fig. 1B, C). As an active endocrine organ, adipose tissue can regulate systemic energy homeostasis by secreting a series of adipokines [28]. Accordingly, we also detected serum leptin and adiponectin, the two important polypeptides secreted by adipocytes, and as expected, the PPA1^{AKO} mice showed significantly decreased serum leptin and adiponectin levels (Fig. 1D). Histological analyses further revealed that brown adipocytes from PPA1^{AKO} mice displayed giant, white adipocyte-like droplets (Fig. 1E) and increased number of smaller adipocytes can be observed in iWAT and eWAT from PPA1^{AKO} mice (Fig.1F, H). The quantification result showed that the average cell size was significantly decreased in both iWAT and eWAT in the PPA1^{AKO} mice (Fig. 1G, I). Besides the average size, we further quantified the cell size distribution and found that the proportion of the very small fat cells, which may contribute to impaired lipid storage capacity, was prominently increased in both iWAT and eWAT (Fig. 1G, I). The above results suggest that deletion of PPA1 may impair adipose tissue development in vivo. Consistent with this, the expressions of genes associated with adipogenesis and lipogenesis, including AP2, Pparγ, AdipoQ, and Fasn, were decreased in both iWAT and eWAT, as shown in Fig. 1J, K. In addition, the protein expression of the mature adipocyte marker AP2, as well as some lipogenic genes such as ACC, FAS, and SREBP1C, was also significantly decreased, as shown in Fig. 1M, N. Similar results were observed in BAT, as both gene and protein expressions of mature brown adipocyte marker UCP1, as well as some adipogenic and lipogenic genes including PPARγ and FAS, were significantly decreased in BAT from PPA1^{AKO} mice (Fig. 1L, O). These observations indicate that PPA1 deletion inhibits the generation of mature, functional adipocytes and results in severe lipodystrophy in vivo.

Adipose PPA1 ablation in mice results in liver steatosis and insulin resistance

The lipodystrophy phenotype prompted us to further examine whether excess lipids had accumulated in other non-adipose tissues. Indeed, we found that the livers of PPA1^{AKO} mice exhibited higher weights and greater lipid accumulation compared with their controls (Fig. 2A–C). Furthermore, liver triglycerides and free fatty acids levels were significantly higher in PPA1^{AKO} mice (Fig. 2D). The genes involved in lipogenesis were also markedly increased in livers from PPA1^{AKO} mice (Fig. 2E, F). Furthermore, insulin sensitivity in the muscle and liver was determined by detecting the insulin signaling transduction. As shown in Fig. 2G, the phosphorylation of Akt (Thr308) and IR (Tyr1150/1151) was significantly attenuated in the liver. Although we did not observe significant repression in IR phosphorylation because of decreased total IR expression, the phosphorylation of Akt was also notably inhibited in the muscle, as shown in Fig. 2H. These findings suggest that insulin sensitivity was substantially blunted in peripheral tissues, including the liver and muscle. Hyperinsulinemia, which may be attributed to decreased insulin sensitivity, was also observed in PPA1^{AKO} mice (Fig. 2I). Intraperitoneal glucose tolerance test (IPGTT) and intraperitoneal insulin tolerance test (IPITT) results further confirmed that PPA1^{AKO} mice exhibited significant glucose intolerance and severe insulin resistance compared to controls (Fig. 2J–K). Furthermore, energy expenditure and substrate utilization were analyzed using a metabolic monitoring system. As shown in Fig. 2L, PPA1^{AKO} mice exhibited significantly increased respiratory exchange ratio (RER) during steady state (the light phase), suggesting a shift in substrate utilization toward carbohydrates relative to fat. Accordingly, we calculated the total rates of fat utilization (Fig. 2M) and carbohydrate utilization (Fig. 2N) for the whole animal [29]. In line with changes in RER, PPA1 deletion in adipose tissue led to a significant decrease in fat utilization, which may be attributed to lipodystrophy. Moreover, the fat mass reduction caused by PPA1 deficiency was more pronounced in aging mice compared with young mice. PPA1 knockout led to a nearly complete lack of both WAT and BAT in aging (10-month-old and 18-month-old) PPA1^{AKO} mice (Fig. S2A–C), resulting in almost undetectable serum adipokines such as adiponectin and leptin (Fig. S2D), as well as significantly impaired insulin sensitivity (Fig. S2E). More importantly, the lipodystrophy in PPA1^{AKO} mice affected the survival rate significantly, as shown in Fig. S2F. Taken together, these data demonstrate that ablation of PPA1 in adipose tissue leads to lipodystrophy, exacerbates liver steatosis, and ultimately results in metabolic complications.

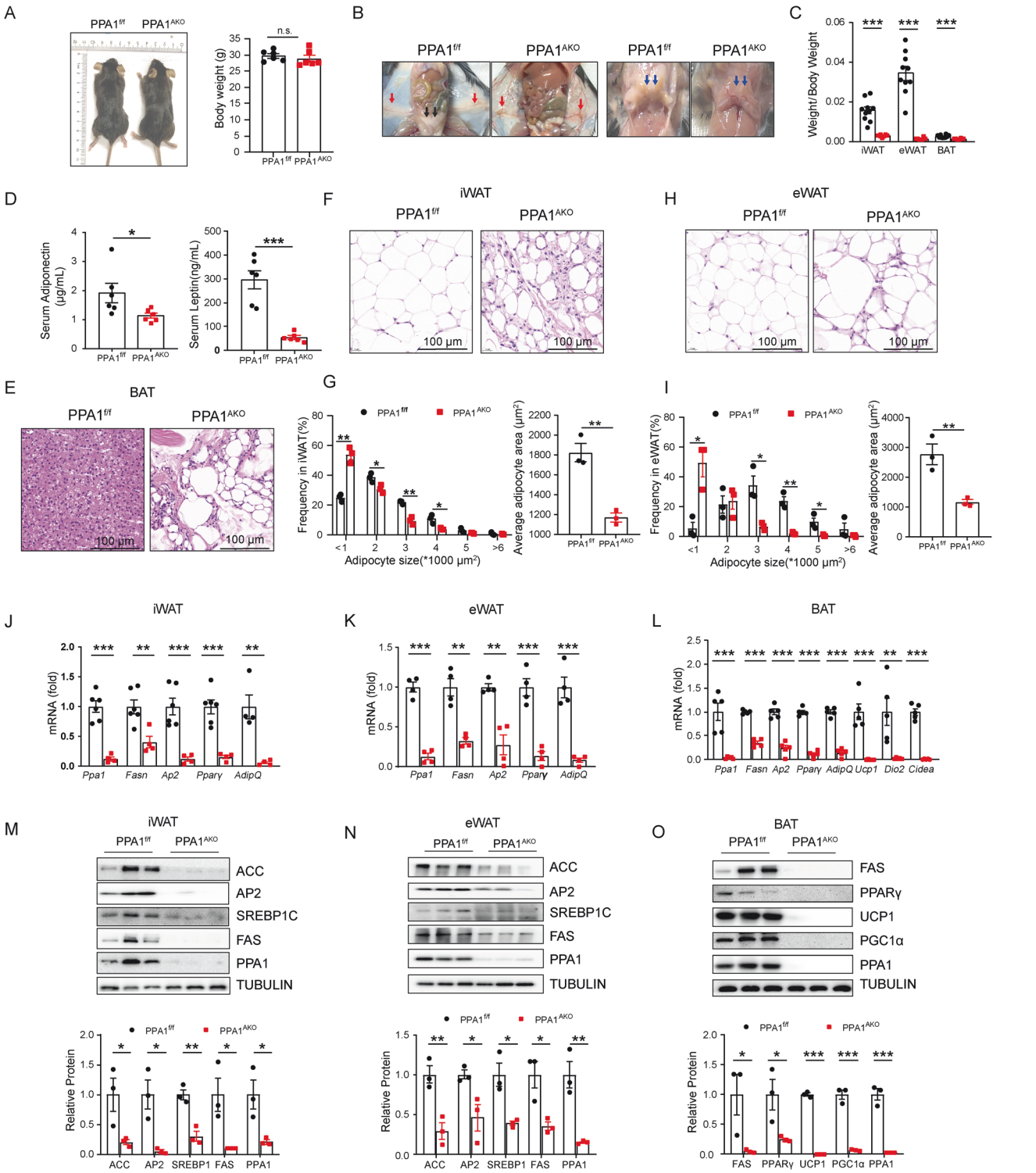

Fig. 1 PPA1 ablation results in severe lipodystrophy in vivo. A Appearance (Left) and body weight (Right) of 3-month-old PPA1^{AKO} and PPA1$^{f/f}$ mice ($n = 6$). **B** Appearance of inguinal WAT (iWAT) and brown fat tissues (BAT) from PPA1^{AKO} and PPA1$^{f/f}$ mice. **C** Weight of iWAT, eWAT and BAT to body weight ratio from PPA1^{AKO} and PPA1$^{f/f}$ mice ($n = 10$). **D** Serum levels of adiponectin and leptin of PPA1^{AKO} and PPA1$^{f/f}$ mice ($n = 6$). **E**, **F**, **H** H&E staining of BAT (**E**), iWAT (**F**), eWAT (**H**) of PPA1^{AKO} and PPA1$^{f/f}$ mice, scale bar=100 μm. **G**–**I** Measurement of adipocyte area of iWAT (**G**) and eWAT (**I**) from PPA1$^{f/f}$ and PPA1^{AKO} mice. The pictures of each section (3 sections/ per group) were obtained and the area of at least 1000 adipocyte cells from each group was analyzed using Pannoramic Viewer. *$p < 0.05$, **$p < 0.01$ compared with PPA1$^{f/f}$ mice. **J**–**L** Relative mRNA expressions of mature white adipocyte markers in iWAT (**J**), eWAT (**K**) and BAT (**L**) of PPA1^{AKO} and PPA1$^{f/f}$ mice ($n = 4$–6). **M**–**O** Western blot analysis of adipogenesis- and lipogenesis-related proteins in iWAT (**M**), eWAT (**N**) and BAT (**O**) of PPA1$^{f/f}$ and PPA1^{AKO} mice (top) and the quantification of protein levels after normalization to TUBULIN (bottom) ($n = 3$). Data are representative of three independent experiments. Data are represented as mean ± SEM. *$p < 0.05$, **$p < 0.01$, ***$p < 0.001$ compared with PPA1$^{f/f}$ mice.

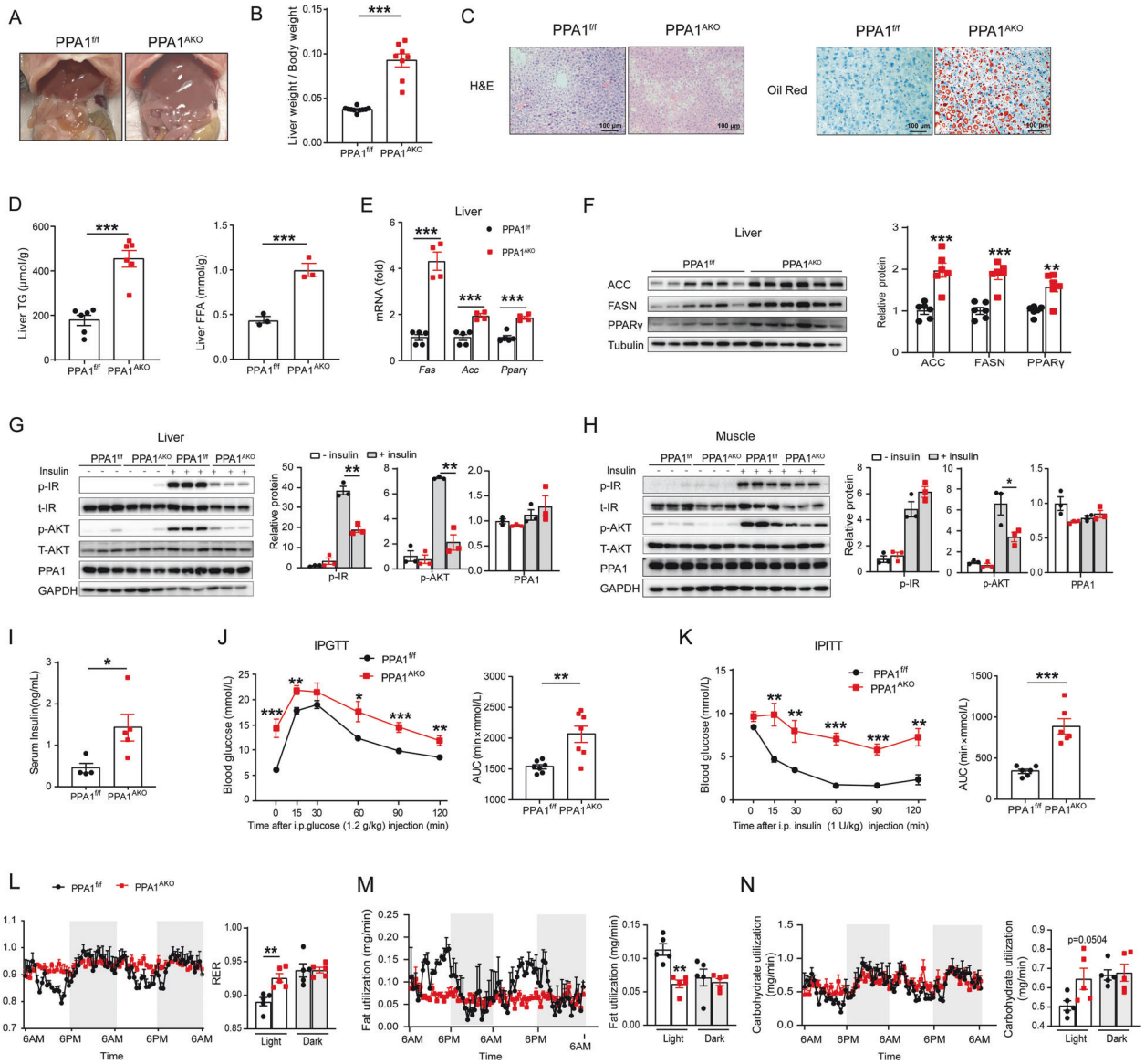

Fig. 2 Adipose PPA1 ablation in mice resulted in liver steatosis and insulin resistance. A Appearance of liver from PPA1^{AKO} and PPA1$^{f/f}$ mice. **B** Liver weight to body weight ratio of PPA1^{AKO} and PPA1$^{f/f}$ mice ($n = 8$). **C** H&E staining and Oil Red O staining of liver of PPA1^{AKO} and PPA1$^{f/f}$ mice, scale bar=100 μm. **D** Total TG ($n = 6$) and FFA ($n = 3$) levels in liver of PPA1^{AKO} and PPA1$^{f/f}$ mice. Q-PCR (**E**) and western blot (**F**) analysis of related gene expression and the quantification of protein levels after normalization to TUBULIN (right) in liver of PPA1^{AKO} and PPA1$^{f/f}$ mice ($n = 4$–6). **G**, **H** Insulin (1.2 U/kg) was injected via inferior vena cava after overnight fasting, tissue samples were collected before (insulin-) or 5 minutes after insulin stimulation (insulin +). Phosphorylation of IR (Tyr1150/1151) and Akt (Thr308) as well as PPA1 levels were detected in liver (**G**) and muscle (**H**) by Western blot and further quantified by normalization to total IR or AKT or GAPDH, respectively (right) ($n = 3$). **I** Serum insulin level of PPA1^{AKO} and PPA1$^{f/f}$ mice ($n = 4$–5). **J** Glucose tolerance test and AUC of 3-month-old PPA1^{AKO} and PPA1$^{f/f}$ mice ($n = 7$). **K** Insulin tolerance test and AUC of 3-month-old PPA1^{AKO} and PPA1$^{f/f}$ mice ($n = 6$). **L–N**: Calculated RER (**L**), fat utilization (**M**) and carbohydrate utilization (**N**) of 3-month-old PPA1^{AKO} and PPA1$^{f/f}$ mice ($n = 5$). Data are representative of three independent experiments. Data are represented as mean ± SEM. *$p < 0.05$, **$p < 0.01$, ***$p < 0.001$ compared with PPA1$^{f/f}$ mice.

PPA1^{AKO} mice are resistant to high-fat-diet (HFD)-induced obesity but develop more severe metabolic disorders

To further assess the effect of PPA1 deficiency on whole-body homeostasis, PPA1^{AKO} and control mice were fed with HFD for 12 weeks. Compared with PPA1$^{f/f}$ mice, HFD-induced weight gain was significantly decreased in PPA1^{AKO} mice (Fig. 3A, B). Anatomical analysis revealed that HFD exacerbated the lipodystrophy caused by absence of PPA1, as the PPA1^{AKO} mice showed markedly reduced masses of iWAT, eWAT, and BAT, as well as dramatically increased liver weight, as shown in Fig. 3C, D. Fewer mature white and brown adipocytes (Fig. 3E), as well as undetectable levels of serum adipokines (Fig. 3F), were observed in the HFD-fed PPA1^{AKO} mice. Although mutant mice were resistant to HFD-induced obesity, PPA1^{AKO} mice exhibited more severe insulin resistance than the PPA1$^{f/f}$ mice administered with an HFD (Fig. 3G). Unexpectedly, we found significantly decreased blood glucose levels after glucose injection in PPA1^{AKO} mice (Fig. 3H). To better determine the possible reason for this effect, the urine glucose was detected after glucose injection. The result revealed that the urine glucose level was increased in PPA1^{AKO} mice, suggesting that part of the glucose may be excreted through urine because of the reduced threshold for renal glucose reabsorption (Fig. 3I). This was further confirmed by providing the mice with drinking water containing 10% glucose for 24 h and

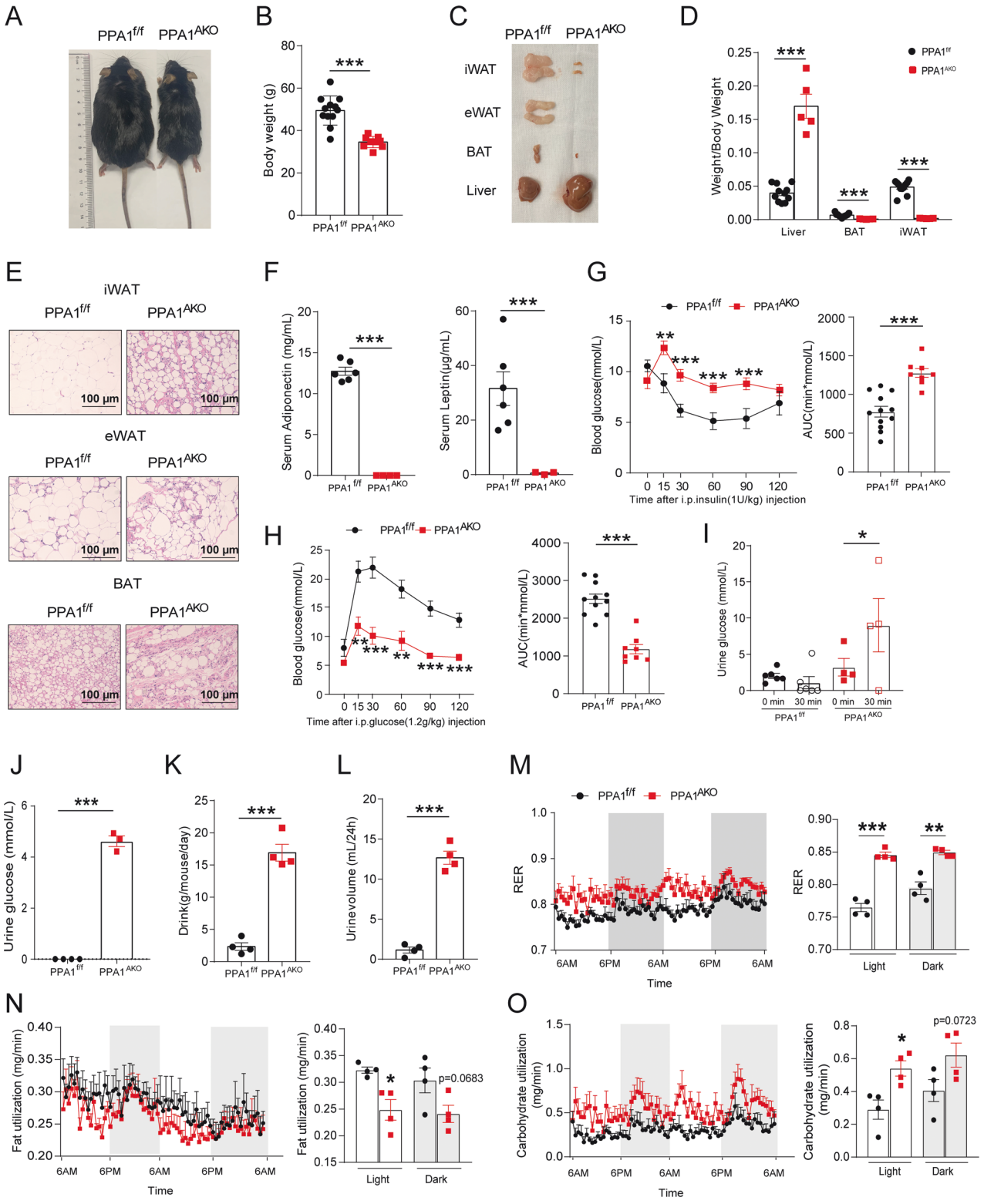

collecting their urine in metabolic cages [30]. Consistently, we observed a profound increase in urinary glucose excretion in PPA1^{AKO} mice compared with the WT mice (Fig. 3J). In addition, excessive urination accompanied by increased water consumption was observed in the PPA1^{AKO} mice (Fig. 3K, L). The increased RER, repressed fat utilization, and enhanced glucose utilization were observed in PPA1^{AKO} mice suggest a shift in substrate utilization as an adaptation to the impaired ability to use fat as an energy fuel (Fig. 3M–O), which may partly contribute to the decreased glucose level observed in the glucose tolerance test (GTT).

PPA1 is required for adipocyte differentiation in vitro

Given the importance of PPA1 on adipose tissue development, we further investigated its effect on adipocyte differentiation in vitro.

Fig. 3 PPA1^{AKO} mice are resistant to HFD-induced obesity but developed more severe metabolic disorders. 4-week-old PPA1^{AKO} and PPA1$^{f/f}$ mice were subjected to a HFD for 12 weeks, and metabolic parameters were detected. **A** Representative pictures of PPA1^{AKO} and PPA1$^{f/f}$ mice. **B** Body weight of PPA1^{AKO} and PPA1$^{f/f}$ mice after HFD feeding ($n = 9$–12). **C** Appearance of iWAT, eWAT, BAT and liver from PPA1^{AKO} and PPA1$^{f/f}$ mice. **D** Weight of iWAT, BAT and liver to body weight ratio from PPA1^{AKO} and PPA1$^{f/f}$ mice, ($n = 5$–11). **E** H&E staining of iWAT, eWAT and BAT of PPA1^{AKO} and PPA1$^{f/f}$ mice, scale bar=100 μm. **F** Serum levels of adiponectin and leptin of PPA1^{AKO} and PPA1$^{f/f}$ mice ($n = 6$). **G** Insulin tolerance test and AUC of PPA1^{AKO} and PPA1$^{f/f}$ mice ($n = 8$–12). **H** Glucose tolerance test and AUC of PPA1^{AKO} and PPA1$^{f/f}$ mice ($n = 8$–11). **I** After overnight fasting, urine glucose levels in PPA1^{AKO} and PPA1$^{f/f}$ mice were measured before or 30 min after intraperitoneal injection of D-glucose (1.2 g/kg) ($n = 4$–6). **J** PPA1^{AKO} and PPA1$^{f/f}$ mice were provided with 10% glucose in drinking water for 24 h and the total volume of urine was collected in metabolic cages. Urine glucose levels were measured ($n = 3$–4). **K**, **L** Metabolic cage monitoring of 24-hour drinking water (**K**) and urine volume (**L**) ($n = 4$). **M**–**O** Calculated RER (**M**), fat utilization (**N**) and carbohydrate utilization (**O**) PPA1^{AKO} and PPA1$^{f/f}$ mice ($n = 4$). Data are represented as mean ± SEM. *$p < 0.05$, **$p < 0.01$, ***$p < 0.001$ compared with PPA1$^{f/f}$ mice.

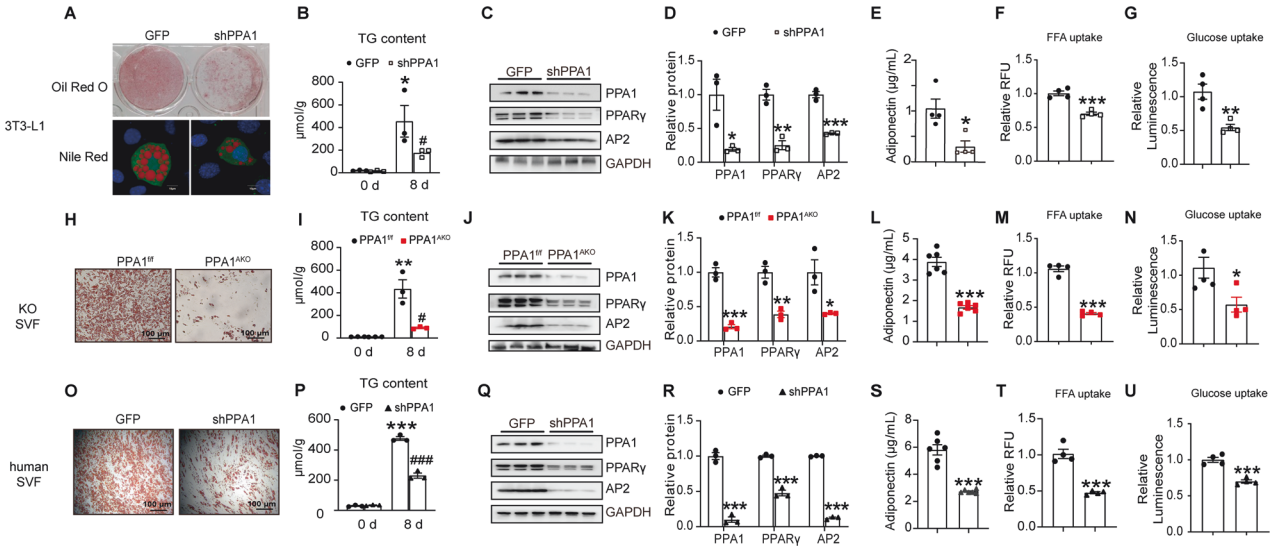

Fig. 4 PPA1 is required for adipocyte differentiation in vitro. A–**G** 3T3-L1 preadipocytes were infected with lentiviral vector expressing control (GFP) or PPA1 knockdown (shPPA1) shRNAs, cells were induced differentiation 2 days later and collected at indicated days. **A** Representative Oil Red O staining (top) and Nile Red staining (bottom) of differentiated cells on day 8 ($n = 3$), scale bar = 10 μm. **B** The TG accumulation was measured on day 0 and day 8 ($n = 3$). **C**, **D** Western blot analysis of adipogenesis-related proteins in GFP and shPPA1 adipocytes on day 8 (**C**) and the quantification of protein levels after normalization to GAPDH (**D**) ($n = 3$). *$p < 0.05$, **$p < 0.01$, ***$p < 0.001$ compared with GFP. E: Adiponectin levels were determined in conditioned media ($n = 4$). *$p < 0.05$ compared with GFP. The uptake assay with labeled fatty acids (**F**) and glucose (**G**) was performed in differentiated GFP or shPPA1 adipocytes ($n = 4$). **$p < 0.01$, ***$p < 0.001$ compared with GFP. **H**–**N** SVF cells isolated from 4-week-old PPA1$^{f/f}$ and PPA1^{AKO} mice iWAT pads were cultured and differentiated into mature adipocytes. Same experiments were performed to determine the effect of PPA1KO on mouse adipocyte differentiation as described in A-G ($n = 3$–6). **O**–**U** SVF cells isolated from human subcutaneous WAT were cultured and infected with GFP or shPPA1, further differentiated into mature adipocytes. Same experiments were performed to determine the effect of PPA1 silencing on human adipocyte differentiation as described in **A**–**G** ($n = 3$–6). Data are representative of three independent experiments. Data are represented as mean ± SEM.

3T3-L1 preadipocytes, which recapitulate major transcriptional events leading to the maturation of adipocytes, were used. Sh-PPA1 was infected into 3T3-L1 preadipocyte before differentiation, and interference of PPA1 strongly inhibited adipogenesis and TG accumulation, as shown in Fig. 4A, B. Concomitantly, the protein expressions of adipogenesis markers accompanied by adipocyte differentiation were significantly inhibited in PPA1 knockdown cells (Fig. 4C, D). Adiponectin secretion was also differentially downregulated, suggesting impaired adipocyte function, as shown in Fig. 4E. The ability of mature adipocytes to efficiently take up free fatty acids (FFA) plays an important role in maintaining lipid homeostasis and is critical to their physiological functions in energy storage. Consistently, FFA uptake was significantly inhibited in adipocytes with PPA1 interference (Fig. 4F). In addition, adipocytes with PPA1 deletion also showed an impaired ability to respond to the insulin-stimulated glucose uptake, as shown in Fig. 4G. These results collectively suggest an essential role of PPA1 in adipocyte differentiation. To confirm the role of PPA1 in adipocyte differentiation and function maintenance, similar studies were performed on primary preadipocytes. Stromal Vascular Fraction (SVF) cells were isolated from iWAT of PPA1$^{f/f}$ and PPA1^{AKO} mice and sub-cultured in vitro. To define the adipose-derived stem cells (ASC) in SVF, two positive markers and two negative cell surface markers were assessed. As shown in Fig. S3A, CD29 and CD90 were expressed in 99% of the cells, whereas CD45 and CD31 were not expressed, indicating a relatively homogenous population of cells. Similarly, human SVF cells were isolated, sub-cultured, and characterized for the presence of ASC (Fig. S3B). Consistent with the results from 3T3-L1 cells, PPA1 knockdown significantly inhibited adipogenesis and cell function in primary preadipocytes from mice (Fig. 4H–N) and human (Fig. 4O–U). The above results indicate the importance of PPA1 in adipocyte differentiation and function.

PPA1 may promote adipocyte differentiation independent of its enzymatic activity

To determine whether the enzymatic activity of PPA1 is essential for adipogenesis, a plasmid express mutant form of PPA1 was constructed via site-specific mutagenesis. The sequence of the active center is strictly conserved and has been well-studied previously [31, 32]. As shown in Fig. 5A, two amino acids, Lys57 and Arg79, which are essential for the enzymatic activity of PPA1, have been mutated. The in vitro tests showed that the PPi hydrolysis activity of the PPA1 mutant has been eliminated

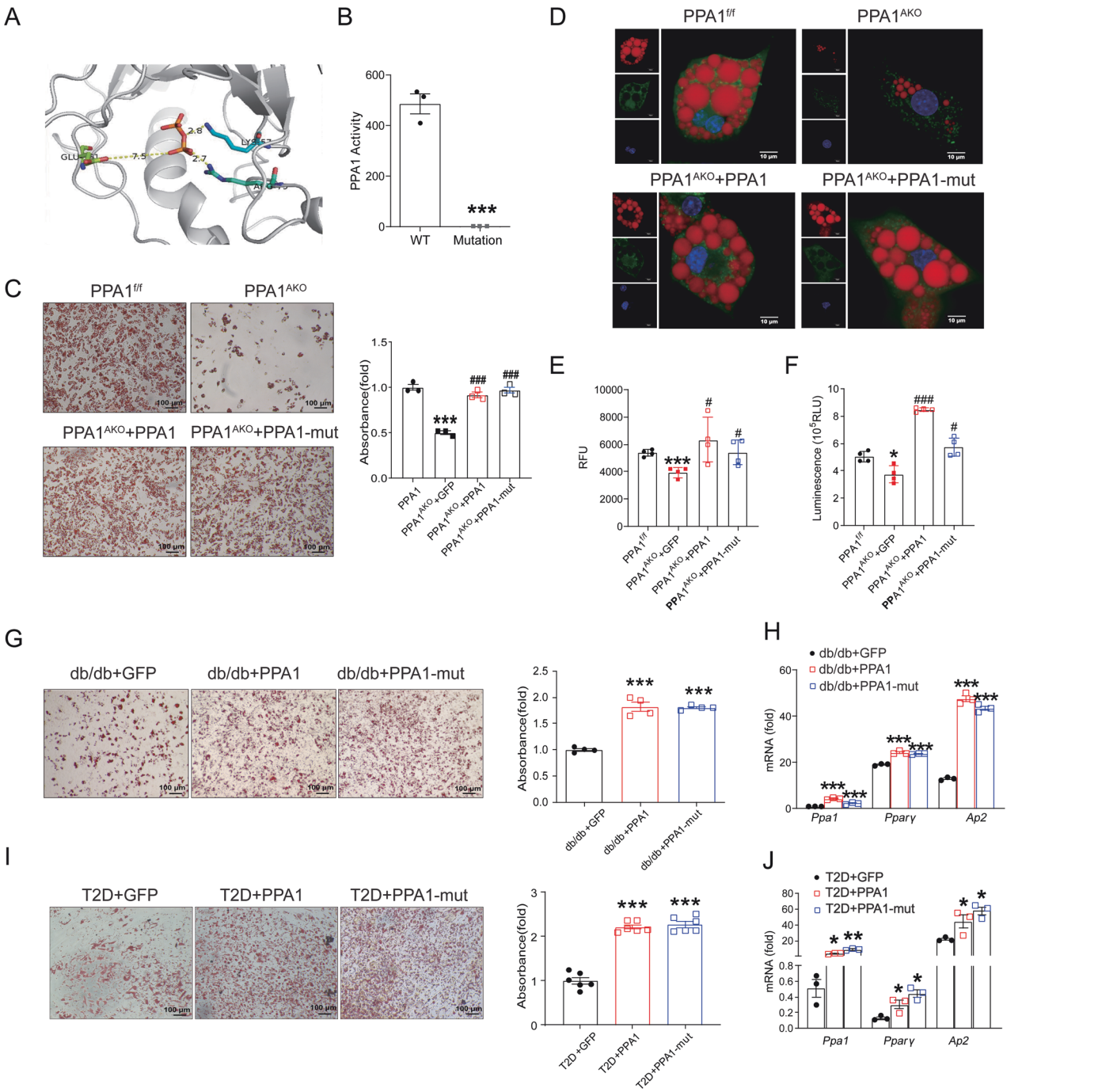

Fig. 5 PPA1 may promote adipocyte differentiation independent of its enzymatic activity. A Three-dimensional structure of the enzymatic active center of PPA1. **B** The enzymatic activity of PPA1 (WT) and PPA1 mutant (Mutation) ($n = 3$). ***$p < 0.001$ compared with WT. **C**–**F** SVF cells were isolated from PPA1$^{f/f}$ and PPA1^{AKO} mice iWAT pads and infected with adenovirus overexpressing GFP (PPA1^{AKO} + GFP), PPA1 (PPA1^{AKO} + PPA1) or PPA1 mutant (PPA1^{AKO} + PPA1-mut), cells were induced differentiation 2 days later and differentiated for 8 days. **C** Representative Oil Red O staining of differentiated cells and relative absorbance ($n = 3$). ***$p < 0.001$ compared with PPA1$^{f/f}$, ###$p < 0.001$ compared with PPA1^{AKO} + GFP, scale bar=100 μm. **D** Nile Red (Red), Hoechst (blue) and lentiviral GFP/shPPA1 (green) staining of in vitro differentiated PPA1$^{f/f}$, PPA1^{AKO}, PPA1^{AKO} + GFP, PPA1^{AKO} + PPA1 adipocytes, scale bar=10 μm. The uptake assay with labeled fatty acids (**E**) and glucose (**F**) was performed in differentiated adipocytes, *$p < 0.05$, ***$p < 0.001$ compared with PPA1$^{f/f}$, #$p < 0.05$, ###$p < 0.001$ compared with PPA1^{AKO} + GFP. **G**, **H** SVF cells were isolated from *db/db* mice and infected with adenovirus overexpressing GFP (*db/db* + GFP), PPA1 (*db/db* + PPA1) or PPA1 mutant (*db/db* + PPA1-mut). Two days later, cells were induced differentiation and collected at day 8. **G** Representative Oil Red O staining of differentiated cells and relative absorbance ($n = 4$), scale bar=100 μm. **H** Relative mRNA expressions of adipogenesis-related genes ($n = 3$). ***$p < 0.001$ compared with *db/db* + GFP. I-J: SVF cells were isolated from T2D patient and infected with adenovirus overexpressing GFP (T2D + GFP), PPA1 (T2D + PPA1) or PPA1 mutant (T2D + PPA1-mut). Two days later, cells were induced differentiation and collected at Day 10. **I** Representative Oil Red O staining of differentiated cells and relative absorbance ($n = 6$), scale bar=100 μm. **J** Relative mRNA expressions of adipogenesis-related genes ($n = 3$). *$p < 0.05$, **$p < 0.01$, ***$p < 0.001$ compared with T2D + GFP. Data are representative of three independent experiments. Data are represented as mean ± SEM.

(Fig. 5B). Therefore, we overexpressed PPA1 or PPA1 mutant in preadipocytes isolated from PPA1$^{f/f}$ and PPA1^{AKO} mice to ascertain whether the effect of PPA1 on adipogenesis is catalytic-dependent. As shown in Fig. 5C, D, adipocyte differentiation was strongly inhibited in preadipocytes isolated from PPA1^{AKO} mice. To our surprise, the overexpression of either PPA1 or PPA1 mutant reversed the repression of adipogenesis and promoted preadipocyte differentiation. More importantly, the overexpression of either the PPA1 or PPA1 mutant can recover the inhibited uptake of lipids and glucose in response to insulin, which can be viewed as indicators of improved adipocyte function (Fig. 5E, F). Impaired preadipocyte differentiation is associated with hypertrophic obesity in type 2 diabetes (T2D) patients according to previous studies [6, 33, 34]. Therefore, we isolated the SVF from *db/db* mice or T2D patients and induced cell differentiation in vitro. As shown in Fig. S4A, C, SVF from *db/db* mice or T2D patients showed inhibited differentiation, as demonstrated by lesser Oil Red staining. The expression of PPA1, together with adipogenesis markers, was also repressed during cell differentiation (Fig. S4B, D). Therefore, we evaluated whether increased expression of PPA1 or PPA1 mutant could promote the differentiation of preadipocytes isolated from T2D models in vitro. As shown in Fig. 5G–J, the repressed adipogenesis of SVF derived from *db/db* mice or T2D patients was reversed by PPA1 overexpression, and the PPA1 mutant showed a comparative effect as that of PPA1. The above results indicate that the function of PPA1 during adipocyte differentiation is independent of its enzymatic activity.

Loss of PPA1 inhibits adipogenesis by promoting C/EBPβ and C/EBPδ degradation

The above data prompted us to explore how PPA1 may affect adipocyte differentiation. 3T3-L1 cells were infected with sh-GFP or sh-PPA1 two days before differentiation and then collected at Day 0, Day 2 and Day 6 for RNA-sequencing (RNA-Seq) analysis. As shown in Fig. 6A, we found the expressions of 2657 genes were already significantly altered from Day 0 to Day 2. Among them, the change in 317 genes was PPA1 dependent. Gene ontology (GO) analysis showed that these PPA1-sensitive genes were associated with cell differentiation and especially correlated with the PPARγ signaling pathway (Fig. 6B), suggesting that PPA1 regulates cell differentiation at the early stage. Consistent with the GO analysis results, quantitative polymerase chain reaction (qPCR) and Western blot showed that both gene expression and protein abundance of PPARγ are significantly decreased when PPA1 is absent (Fig. 6C–E). Alternation of PPA1 expression during 3T3-L1 cell differentiation also suggested that PPA1 may play a key role in early cell differentiation (Fig. 6F). Previous studies have established that activated C/EBPβ, together with C/EBPδ, induces PPARγ and C/EBPα expression to further promote adipogenesis at early stages [35, 36]. Therefore, the protein abundance of C/EBPβ and C/EBPδ was detected, and the result showed significantly decreased C/EBP expression with PPA1 deletion (Fig. 6G, H). Surprisingly, the mRNA level of these two TFs was not affected by PPA1 knockdown (Fig. 6I, J). Moreover, PPA1 deficiency had no effect on cAMP level or cAMP response element-binding protein (CREB) phosphorylation, which directly regulates C/EBPβ transcription (Fig. S5A, B). The mRNA stability of C/EBPβ and C/EBPδ was also evaluated by detecting mRNA abundance after treatment with Actinomycin D, the RNA polymerase inhibitor. As shown in Fig. S6, PPA1 deletion did not affect the mRNA stability of C/EBPβ and C/EBPδ. To further explore whether decreased C/EBP protein abundance was caused by inhibited protein synthesis or increased protein degradation, translation inhibitor cycloheximide (Chx) was used 3 hours after induction. As shown in Fig. 6K, L, the degradation of C/EBPβ and C/EBPδ increased in cells with PPA1 knockdown, confirming that PPA1 affects the stability of C/EBPβ and C/EBPδ. Given that C/EBP family TFs are constitutively multi-ubiquitinated and subsequently degraded by the proteasome [37], 3T3-L1 cells with or without PPA1 deletion were treated by MG132 during differentiation. Results indicated that MG132 treatment was able to overcome the increased C/EBPβ degradation caused by PPA1 deletion (Fig. 6M). To better confirm the effect of PPA1 deletion on C/EBP stability, above-mentioned experiments were further performed on SVF isolated from PPA1$^{f/f}$ and PPA1^{AKO} mice, as shown in Fig. 6N–T. Consistently, we observed decreased C/EBP protein abundance and reduced protein stability in PPA1 deletion cells. Moreover, decreased C/EBPβ and C/EBPδ protein expression was also observed in iWAT from PPA1^{AKO} mice as shown in Fig. 6U.

DISCUSSION

The present study revealed a previously unrecognized role of PPA1 in adipose tissue function and whole-body energy homeostasis. We report that PPA1 is indispensable for full adipogenesis both in vitro and in vivo. Adipose-specific deletion of PPA1 in mice results in impaired adipose tissue development, followed by ectopic lipid accumulation, severe insulin resistance, and metabolic disorders. Mechanistically, we found that PPA1 regulates adipocyte differentiation independent of its PPi catalytic activity. PPA1 can modulate the early phase of adipogenesis by mediating C/EBPβ and C/EBPδ stability through the inhibition of their proteasome-dependent degradation.

Previous studies on PPA1 in mammals predominantly focused on its high expression in several cancer cell lines, where the pyrophosphatase activity of PPA1 has been linked to the growth of several solid tumors [23, 38, 39]. In the current study, we found that adipose-specific PPA1 deficiency led to lipodystrophy followed by metabolic complications, and the reduction of fat mass exacerbated in aging mice. More importantly, reduced survival rates were observed in aging PPA1^{AKO} mice, consistent with the findings in patients with lipodystrophy. Studies have reported accelerated aging and reduced life expectancy in patients with congenital generalized lipodystrophy due to complications of diabetes or liver and heart disease [9, 10]. In addition, the female PPA1^{AKO} mice showed a more pronounced phenotype, characterized by elevated liver weight and an almost complete lack of response to insulin injection (Fig. S7). This can be explained by the fact that female mice generally have a higher percentage of body fat.

Further investigations revealed that the lipodystrophy caused by PPA1 deletion was triggered by impaired adipocyte differentiation. PPA1 emerged as a positive regulator of adipogenesis, with its absence dramatically inhibiting differentiation, while its overexpression significantly promoted it. In a previous study, we demonstrated that PPA1 can work as a PPARγ target gene to maintain mitochondrial biogenesis and function in adipocytes [27]. In this study, we found alterations in PPARγ expression following changes in PPA1 expression, suggesting a positive feedback regulation between PPA1 and PPARγ in adipocytes. Moreover, we noticed that PPA1 expression started to increase in the early phase of differentiation and decreasing to basal level at Day 2. Interestingly, PPA1 expression strongly increased again and stayed high at the terminal stage of differentiation (Fig. 6F). Given that adipogenesis is driven by two distinct waves of TF activation (i.e., C/EBPβ and C/EBPδ in the first wave and C/EBPα and PPARγ2 in the second wave) [40], we silenced PPA1 at different stages to elucidate its role during differentiation. We found that only PPA1 silencing before the initiation of adipocyte differentiation can inhibit adipogenesis and repress the expression of marker genes, whereas silencing PPA1 at the terminal stage (48 hours post-differentiation) exerted limited effects on adipogenesis (Fig. S8). Therefore, our findings indicate that PPA1 specifically regulates the early stage of adipocyte differentiation.

During the early stage, growth-arrested preadipocytes re-enter the cell cycle and undergo MCE after adipogenesis induction. Therefore, we first determined the cell number during MCE, and as

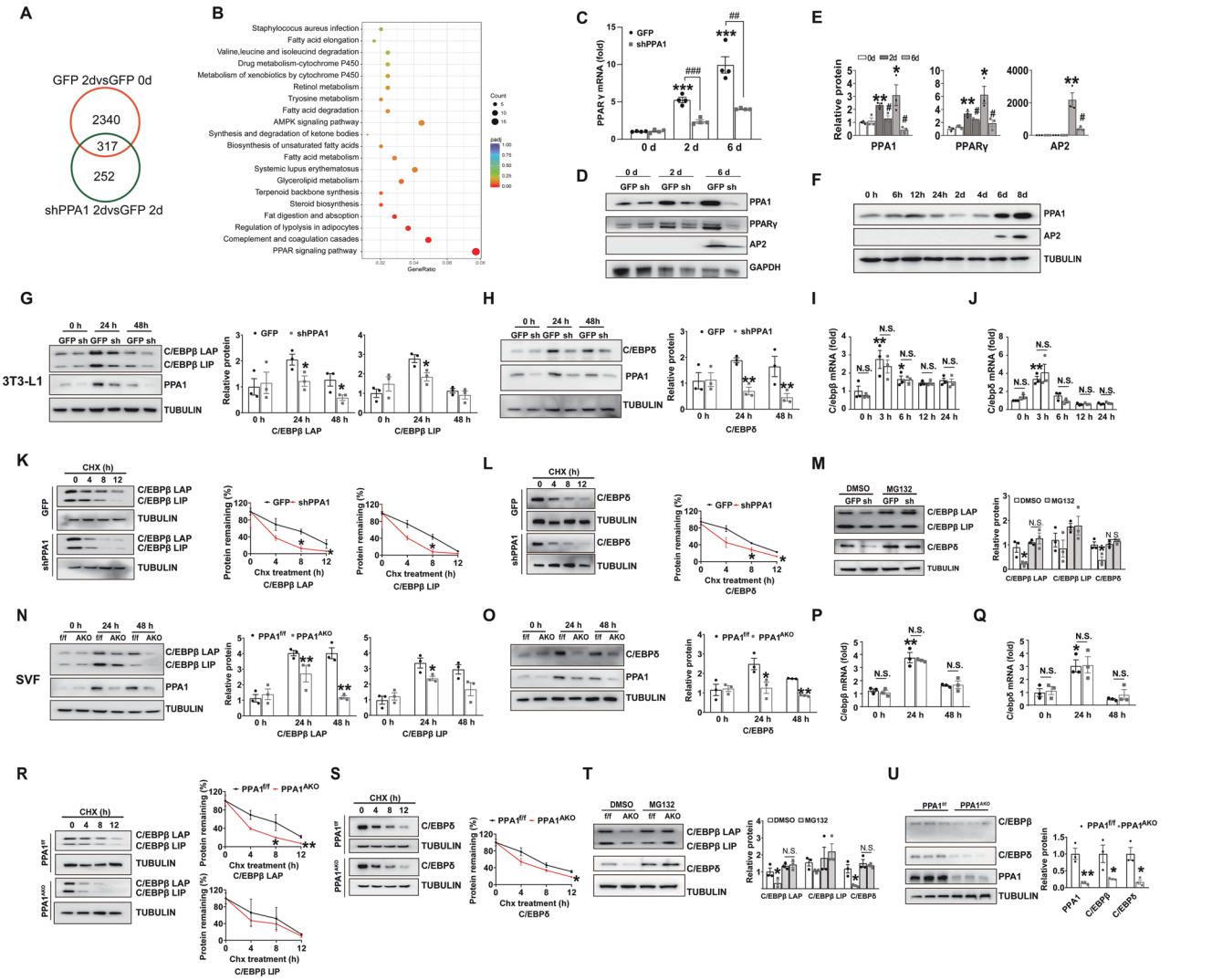

Fig. 6 Loss of PPA1 inhibited adipogenesis through increasing C/EBPβ and C/EBPδ proteasome-dependent degradation. A, **B** Adipogenic transcriptome alternations. **A** Venn diagram depicting adipogenic related genes (2657) and PPA1-sensitive (569) genes at day 2. **B** GO analysis of PPA1-sensitive genes at day 2. **C**–**F** 3T3-L1 preadipocytes were infected with lentiviral vector expressing control (GFP) or PPA1 knockdown (shPPA1) shRNAs, cells were induced differentiation 2 days later and collected at indicated time. **C** Q-PCR analysis of PPARγ gene expression ($n = 4$), ***$p < 0.001$ compared with 0 day GFP, ### $p < 0.001$ compared with 2day GFP, ## $p < 0.01$ compared with 6 day GFP. **D**, **E** Western blot analysis of adipogenic protein level in 3T3-L1 cells differentiated at indicated days (**D**) and the quantification of protein levels after normalization to GAPDH (**E**) ($n = 3$). *$p < 0.05$, **$p < 0.01$ compared with 0 d GFP, # $p < 0.05$ compared with 2 d/6d GFP, respectively. **F** Western Blot analysis of PPA1 expression during 3T3-L1 cell differentiation ($n = 3$). **G**, **H** C/EBPβ LAP and LIP (**G**) and C/EBPδ (**H**) protein level during the first 48 h of differentiation in 3T3-L1 cells were measured by western blot. The quantification of protein levels was normalized to TUBULIN ($n = 3$). *$p < 0.05$, **$p < 0.01$ compared with 24 h/48 h GFP, respectively. **I**–**J** Q-PCR analysis of C/EBPβ (**I**) and C/EBPδ (**J**) gene expression during 3T3-L1 cell differentiation ($n = 3$). *$p < 0.05$, **$p < 0.01$ compared with 0 h. Protein translation inhibitor cycloheximide (CHX, 25 μg/ml) was added 3 hours after induction of differentiation. Western blot analysis of C/EBPβ LAP and LIP (**K**) and C/EBPδ (**L**) at indicated time (0, 4, 8 and 12 h after chx treatment) in 3T3-L1 cells. The quantification of protein levels was normalized to TUBULIN ($n = 3$). *$p < 0.05$ compared with GFP. **M** Proteasome inhibitor MG132 (25 μM) was added 6 hours after induction of differentiation. C/EBPβ and C/EBPδ protein in 3T3-L1 cells were measured by western blot after 12 h treatment with MG132. The quantification of protein levels was normalized to TUBULIN ($n = 3$). *$p < 0.05$ compared with GFP (DMSO). **N**–**T** SVF cells from iWAT pads were isolated from 4-week-old PPA1$^{f/f}$ and PPA1^{AKO} mice and cultured for several days until reaching confluence. Cells were then induced to differentiate and collected at indicated time. C/EBPβ LAP and LIP (**N**) and C/EBPδ (**O**) during the first 48 h of differentiation in SVF cells isolated from PPA1$^{f/f}$ (f/f) and PPA1^{AKO} (AKO) mice were measured by western blot. The quantification of protein levels was normalized to TUBULIN ($n = 3$). *$p < 0.05$, **$p < 0.01$ compared with 24 h/48 h GFP, respectively. Q-PCR analysis of C/EBPβ (**P**) and C/EBPδ (**Q**) gene expression during SVF cell differentiation ($n = 3$). *$p < 0.05$, **$p < 0.01$ compared with 0 h. **R**, **S** Protein translation inhibitor cycloheximide (CHX, 25 μg/ml) was added 3 hours after induction of differentiation. Western blot analysis of C/EBPβ LAP and LIP (**R**) and C/EBPδ (**S**) at indicated time (0, 4, 8 and 12 h after chx treatment) in PPA1^{AKO} SVF cells. The quantification of protein levels was normalized to TUBULIN ($n = 3$). *$p < 0.05$, **$p < 0.01$ compared with PPA1$^{f/f}$. T: Proteasome inhibitor MG132 (25 μM) was added 6 hours after induction of differentiation. C/EBPβ and C/EBPδ protein in PPA1$^{f/f}$ (f/f) and PPA1^{AKO} (AKO) SVF cells were measured by western blot after 12 h treatment with MG132. The quantification of protein levels was normalized to TUBULIN ($n = 3$). *$p < 0.05$ compared with GFP (DMSO). **U** Western blot analysis of C/EBPβ and C/EBPδ in iWAT from PPA1^{AKO} and PPA1$^{f/f}$ mice. The quantification of protein levels was normalized to TUBULIN ($n = 3$). *$p < 0.05$, **$p < 0.01$ compared with PPA1$^{f/f}$. Data are representative of three independent experiments. Data are represented as mean ± SEM.

shown in Fig. S9A, the increase in cell number was significantly inhibited in the absence of PPA1. Previous studies have suggested that progression from G1 to S requires the down-regulation of p27 and the activation of cdk2 in most cell types, including preadipocytes, and that impaired adipogenesis was associated with increased p27 expression during critical periods of differentiation [20, 41]. As shown in Fig. S9B, the absence of PPA1 led to a significant increment of P27 abundance and a marked reduction of CDK2 expression, indicating suppressed MCE caused by PPA1 deletion. Study had reported that PPA1 can enhance cell proliferation in colon cancer cells, but the pyrophosphatase activity is indispensable in their study [21]. So in this study, we also evaluated the effect of PPA1 on cell proliferation by EdU staining in 3T3-L1 cells which were not subjected to differentiation induction. As shown in Fig. S9C, no differences were observed in cell proliferation in PPA1 knockdown cells. Therefore, the inhibited MCE caused by PPA1 deletion in adipocytes mainly results from decreased C/EBPβ expression, which was already well documented in previous studies [42, 43].

Adipogenesis involves a complex network of regulatory proteins, but PPARγ is the master regulator. The expression of PPARγ is positively regulated by a series of TFs, among which C/EBPβ is a pioneer TF during the early phase of adipogenesis [15]. The treatment of hormone inducers triggers a cascade in which C/EBPβ and δ are rapidly expressed, followed by the expression of C/EBPα and PPARγ [11, 44]. Unlike C/EBPδ, which has been reported to possess minimal adipogenic activity alone, C/EBPβ is indispensable in adipocyte differentiation [36]. Knockdown of C/EBPβ blocks adipogenesis, whereas its overexpression is sufficient to induce 3T3-L1 cell differentiation in the absence of hormone inducers [36]. The multiple functions and proper activation of C/EBPβ in adipogenesis are highly regulated by post-transcriptional modifications (PTMs) as well as cross-talks of different types of PTMs [45]. The PTMs of C/EBPβ, including phosphorylation, acetylation, methylation, ubiquitination, and SUMOlation, control not only the transcriptional activity but also the stability of this TF. A previous study has suggested that PIAS1, a SUMO E3 ligase, negatively regulates adipogenesis by promoting C/EBPβ degradation [46]. Conversely, SENP2, the SUMO-specific protease, plays a critical role in adipogenesis by de-SUMOlation and stabilization of C/EBPβ [47]. Previous studies have also documented that the major isoforms of C/EBPβ, LAP, and LIP may exert different effects on adipocyte differentiation; LAP promotes adipogenesis, while the overexpression of LIP has anti-adipogenic activity [48, 49]. In our study, we found both LAP and LIP to be decreased in PPA1 knockdown cells, but the decrease of LAP on the protein level was more prominent than that of LIP (Fig. 6G, N). Similarly, the knockdown of PPA1 had a more profound effect on LAP protein stability compared with LIP (Fig. 6K, R). This can partly be explained by the fact that the proteolytic stabilities of the two C/EBPβ isoforms are different. Although both isoforms are targets of ubiquitin/proteasome-dependent degradation, the abundance of polyubiquitinated derivatives detected for the two isoforms differs in the course of adipogenic differentiation. Unlike LAP, the level of polyubiquitinated LIP significantly increases at later stages during differentiation [49].

In a previous study, PPA1 was suggested to inhibit cell proliferation through direct binding and dephosphorylation of pJNK in cancer cells, but the dephosphorylation activity of PPA1 is still coupled to its PPi catalytic activity [50]. Therefore, we also performed immunoprecipitation–western blot analysis in 3T3-L1 cells with or without differentiation to evaluate whether PPA1 might affect stability through direct interaction with C/EBPβ. However, we did not detect the C/EBPβ protein in PPA1 immunocomplexes (Fig. S10A), suggesting that PPA1's enhancement of C/EBPβ stability does not occur through direct interaction between the two proteins. In addition, immunofluorescence staining revealed no overlap between PPA1 staining and C/EBPβ staining (Fig. S10B). Therefore, it is worthwhile in our further work to clarify the exact mechanism by which PPA1 prevents C/EBP degradation.

Not too long ago, inhibitors of adipogenesis were widely regarded as a good treatment for obesity. However, many studies, from rodents to humans, have demonstrated that limited adipose tissue expansion is associated with insulin resistance and other metabolic abnormalities [9]. Nowadays, an increasing number of studies are beginning to view pathological obesity as a form of relative lipodystrophy, given strong evidence supporting the notion that the inability to expand subcutaneous WAT depots when faced with excess nutrients is detrimental to metabolic health in the obese state [6]. In this study, we also observed decreased adipogenesis of preadipocytes isolated from *db/db* mice and T2D patients, along with inhibited PPA1 expression. Moreover, overexpression of PPA1 can promote adipocyte differentiation in vitro in an enzymatically independent manner. In the future, mice with inducible expression of PPA1 will be further employed to better understand the protective effect of PPA1 under conditions of over-nutrition.

In conclusion, the results from this study demonstrated, for the first time, the essential roles of PPA1 in adipogenesis. Our observations revealed that PPA1 functions as a positive regulator of adipocyte differentiation by increasing C/EBPβ and C/EBPδ stability in an enzymatically independent manner, a mechanism that has not been previously reported. Given the vital role of PPA1 in the C/EBPβ-PPARγ axis, targeting PPA1 may hold promise as a potential therapy for ameliorating obesity-related metabolic disorders.

MATERIALS AND METHODS

Reagents

Collagenase Type I (#C0130), Dexamethasone (#D4902), 3-Isobutyl-1-methylxanthine (IBMX) (#I7018), Insulin (#I5500) and Nile Red (#72485) were from Sigma-Aldrich (St. Louis, MO, USA). SYBR Green Mix (#Q111-02), RT-PCR kit (#R222-01-AB) were from Vazyme Biotech Co.,Ltd (Nanjing, China). Protease inhibitor cocktails (Cat#11697498001) were from Roche Ltd. (Switzerland). Cycloheximide (CHX) (#HY-12320), MG-132 (#HY-13259), actinomycin D (#HY-17559) were from MedChemExpress express Co.,Ltd (Shanghai, China). DMEM, DMEM/F12, fetal bovine serum (FBS), newborn calf serum (CBS) was from Gibco (USA).

Animals

PPA1 floxed mice ($PPA1^{f/f}$) were generated at Cyagen Biosciences (Suzhou, China) at the background of C57/BL6J. Adipose-specific PPA1 knockout mice (herein referred to as $PPA1^{AKO}$ mice) were generated by crossing $PPA1^{f/f}$ with Adiponectin-Cre mice (Jackson Laboratories). Mice were randomly assigned to experimental groups. For HFD treatment, 4-week-old male mice were fed with diet containing 60% fat-derived calories (Research Diets, #D12492) for 12 weeks. Genetically diabetic leptin receptor-mutated (*db/db*) mice and their littermate control (*db/ctrl*) were purchased from the Jackson Laboratory. Mice were housed in a specific pathogen-free facility with a temperature and humidity controlled environment (23°C, 12-hour light/dark cycle, 60–70% humidity) at Nanjing Medical University, with free access to commercial rodent chow and tap water. All procedures concerning the animal care and use were in accordance with the guidelines of the Institutional Animal Care and Use Committee of the Nanjing Medical University, China (Permit Number: IACUC-NJMU 14030178).

Glucose tolerance test (GTT) and insulin tolerance test (ITT)

For GTTs, mice were intraperitoneally (i.p.) injected with D-glucose (1.2 g/kg) after 14 hours of fasting, and tail blood glucose level was monitored at 0, 15, 30, 60, 90 and 120 min after glucose injection. For ITTs, mice were i.p. injected with insulin (1 U/kg for mice fed on a chow diet and 1.2 U/kg for mice fed with HFD) after 6 hours of fasting. Blood glucose was measured at 0, 15, 30, 60, 90,120 min after insulin injection.

Experiments involving measurements of blood glucose and body weight of mice were performed in a blinded fashion, with randomly grouped mice based on their toe clipping numbers.

Serum metabolic parameters

Blood samples were collected from mice in fasted conditions and centrifuged for 15 min at 3,500 rpm. Commercially available kits were used to measure plasma levels of insulin (EZassay, MS200); adiponectin (Millipore, EZMADP-60K); leptin (R&D, MOB00); triglycerides (APPLYGEN, E1013) and free fatty acids (WAKO, 294-63601), respectively.

Metabolic measurements in vivo

The comprehensive metabolic phenotypes of mice were assessed using the automated home-cage system (PhenoMaster, TSE). All mice were single housed in the metabolic chambers with food and tap water provided *ad libitum*. Before the experiments, mice were acclimated in the metabolic chambers for 2 days. Metabolic parameters including oxygen consumption, CO_2 generation, and respiratory exchange ratio were monitored and recorded every 40 min for 5 consecutive days. Whole-body fat utilization was calculated using the following equation: $1.67 \times (VO_2 - VCO_2)$. Whole-body carbohydrate utilization was calculated using the following equation: $4.55 \times VCO_2 - 3.21 \times VO_2$ [29]. For the measurement of urine glucose levels, an extra assessment was performed on the HFD $PPA1^{AKO}$ and $PPA1^{f/f}$ mice. Mice were provided with 10% glucose in drinking water for 24 h in metabolic cages. 24 h water and 24 h urine volume was recorded, and urine specimens were collected for analysis.

Morphometric and histologic analysis

Adipose tissue and liver sections isolated from mice were fixed overnight in 4% paraformaldehyde. Samples were processed for paraffin embedding, sectioning, and H&E staining. For liver Oil Red O staining, frozen liver tissues from $PPA1^{f/f}$ and $PPA1^{AKO}$ mice were embedded in Tissue-Tek O.C.T. compound and cryosectioned in 15 μm slices at −20 °C using a CryoStar NX50 microtome (Thermo-Scientific, Germany). Liver sections were then stained with Oil Red O. Microphotographs were taken by Olympus microscope. Adipocyte size measurement was performed according to the procedure as described [51]. In brief, the adipocyte sizes were measured by manual counting of cells on H&E slides from at least three fields of three mice per group utilizing the Pannoramic Viewer software from the Digital Pathology Company.

Cell culture and differentiation

3T3-L1 cell line (#CL-173, ATCC) was cultured in high-glucose DMEM supplemented with 10% newborn calf serum and 1% penicillin/streptomycin at 37 °C and in a humidified atmosphere containing 5% CO_2. For adipocyte differentiation, post-confluent cells (defined as day 0) were cultured for 2 days in DMEM medium containing 10% fetal bovine serum, 1% penicillin/streptomycin supplemented with 1 μg/ml insulin, 1 μM dexamethasone, 0.5 mM 3-isobutyl-1-methylxanthine. After 2 days, medium was replaced with maintenance medium containing 1 μg/ml insulin. Thereafter, the medium was replaced every 2 days until the cells were fully differentiated.

Isolation of stroma-vascular fraction (SVF) cells from the inguinal WAT was performed as previously described [52]. Briefly, freshly isolated iWAT pads from 4-week-old $PPA1^{AKO}$ mice, *db/db* mice and their control littermates (5 mice/per group) were minced into pieces with scissors and digested in collagenase type I (2 mg/ml) for 45 min at 37 °C water bath with gentle shaking. The digested homogenates were passed through a 70-μm cell strainer (BD Biosciences) to remove undigested tissues, followed by centrifugation at 1000 rpm for 10 min at RT. Pellets containing SVF cells were washed with PBS by centrifugation at 1000 rpm for 10 min. The SVF which contains ASCs, was then plated in warm culture medium (DMEM with 10% FBS and 1% penicillin/streptomycin) in a 10-cm dish for 2 hours and then gently washed with culture media to remove cell debris and non-adherent cells, thus enriching for ASCs which adhere well to the culture surface (designated as Passage 0). Then SVF cells (designated as day 0) were cultured in the induction media containing 1 μg/ml Insulin, 1 μM Dexamethasone, 0.5 mM 3-isobutyl-1-methylxanthine for two days, and then the cells were cultured in maintenance medium containing 1 μg/ml Insulin. Thereafter, the medium was replaced every 2 days until the cells were fully differentiated.

Human SVF isolation and differentiation

Human samples consisting subcutaneous adipose tissues were from 6 individuals with Type 2 Diabetes and 6 healthy individuals who underwent surgery in Southeast University Affiliated Zhongda Hospital during 2020–2022 (Permit number: 2020ZDSYLL144-P01 by the Independent Ethics Committee of Southeast University Affiliated Zhongda Hospital). The patients had signed written consent before surgery. Biopsies were placed on ice and SVF cells were immediately isolated as previously reported [53]. Briefly, freshly isolated adipose tissues were minced and digested in DMEM/F12 containing collagenase type I (2 mg/ml) and BSA (35 mg/ml) for 40 min at 37 °C in the water bath with gentle shaking. Following digestion, FBS was added to stop Collagenase thoroughly. The homogenates were filtered through a 70-μm cell strainer and spun down at 300 g for 10 minutes. Most of the floating supernatant were aspirated off and pellets were resuspended and washed in DMEM/F12 by centrifugation for 10 min at 300 g for 2 times. The pellets were then plated in warm culture medium (DMEM with 10% FBS and 1% penicillin/streptomycin) in a 10-cm dish for 2 hours and then gently washed with culture media to remove cell debris and non-adherent cells. The medium was replaced every second day until the cells reached 80% confluence. Subsequently, cells were cryopreserved from each sample (approximately 1 tube of 5×10^6 cells) and frozen in liquid nitrogen until analyses.

For differentiation experiments, different groups of cells were thawed and seeded in 6-well culture plates in culture medium. The medium was changed every two days until the cells reached complete confluency. Then cells were replaced with serum-free induction medium consisting of DMEM/F12, supplemented with 1 μM Rosiglitazone, 1 μM Insulin, 0.5 mM 3-isobutyl-1-methylxanthine, 1 μM Dexamethasone for 2 days, and then the cells were cultured in maintenance medium containing 1 μM Insulin. Thereafter, the medium was replaced every 2 days until the cells were fully differentiated.

Flow cytometry

The cell surface markers of SVF from mice (Passage 1) were measured using a FACScan flow cytometer (BD, USA) using fluorochrome-conjugated antibodies, including CD29-PE (1 μg/test; 12-0291-81, eBiosciences), CD90-PE (0.25 μg /test; 12-0909-41, eBiosciences), CD45-FITC (0.5 μg/test; 11-0451-82, eBiosciences), and CD31-FITC (1 μg /test; 11-0311-82, eBiosciences); The cell surface markers of SVF from human adipose tissues (Passage 2-3) were measured using fluorochrome-conjugated antibodies, including CD90-FITC (1 μg /test; 11-0909-42, eBiosciences) and CD45-FITC (0.25 μg/test; 11-0459-42, eBiosciences).

Cell adenovirus infection and lentivirus transduction

The adenovirus-mediated PPA1, mutPPA1, CMV Cre-specific overexpression was constructed by Genomeditech Ltd (Shanghai, China). The adenovirus was transfected into SVF cells 2 days before differentiation. The lentivirus-mediated PPA1-specific small hairpin RNA (shPPA1) were performed as previously described [27]. The lentivectors containing the shRNA sequences were transfected into 3T3-L1 cells 2 days before differentiation.

Adipocyte Oil-Red-O staining

Oil Red O (0.5% (w/v) in isopropanol) was diluted with water (3:2), filtered through a 0.45 μm filter. Differentiated cells were washed 3 times with PBS and fixed for 10 min with 4% paraformaldehyde (PFA), then the fixed cells were incubated with filtered Oil Red O for 1 h at RT. For quantification, Oil Red O was extracted by incubating dried samples stained on the same day in 100% isopropanol for 5 min at room temperature and absorbance was measured at 510 nm.

Adipocyte Nile-Red staining

Differentiated cells were stained with Nile Red (0.1 μg/mL) and Hoechst 33342 for 20 min at cell incubator. Images were captured by a confocal scanning fluorescence microscope (FV1200, Olympus, Japan).

Fatty acid and glucose uptake assay

Differentiated adipocytes were seeded in 96-well plates at a density of 5*10^5 cells/per well. Fatty acid uptake in cells were determined using a commercial assay kit (Abnova, KA4084). Glucose uptake in cells were determined using a commercial assay kit (Cayman, 600470).

Determination of tissue and cell lipids

Triglycerides (TG) and FFA contents in tissues or cells were measured with commercial kits from APPLYGEN (#E1013) and WAKO (#294-63601) respectively.

RNA stability assay

To detect the mRNA stability of C/EBPβ and C/EBPδ, 3T3-L1 cells differentiated for 3 hours were treated with actinomycin D (2 mg/ml final concentration) and RNA was harvested at different time points (0, 30, 90, 120 and 150 min post-actinomycin D treatment) followed by cDNA

synthesis and reverse transcription quantitative PCR analysis (RT-qPCR). Primers are listed in Supplementary Table 1.

3T3-L1 cells cAMP assay

3T3-L1 preadipocytes were infected with lentiviral vector expressing control (GFP) or PPA1 knockdown shRNAs (shPPA1) and seeded at 10^4 cells/well in a 96-well plate, respectively. Then the cAMP levels of cells at 0, 1, 3, 6 h post differentiation were detected using a competitive cAMP Assay kit (Abcam 65355).

PPase activity assay

The recombinant protein expression of PPA1 (WT) and PPA1 mutant (PPA1 mutation) was induced by 0.4 mM IPTG and purified via the Nickel affinity chromatography. Then protein was dissolved to a working concertation in 1 μM with the mixture buffer of 100 mM Tris-HCl containing 3 mM $MgCl_2$ and glycerol. The enzyme activity of WT and PPA1 mutation was detected by in vitro enzyme activity test. Detailed experimental procedures and analysis methods are as previously described [54].

RNA isolation and qPCR

Total RNA was isolated using the Trizol reagent. The first-strand cDNA synthesis was performed using 1 μg total RNA. Quantitative RT-PCR was performed using the SYBR Green PCR Master Mix and LightCycler480 II Sequence Detection System (Roche, Switzerland). The relative expression levels were determined using the $2^{\Delta\Delta CT}$ method and normalized to the internal control gene arpppo. Primer sequences were provided in Table S1.

RNA-Seq analysis

3T3-L1 preadipocytes were infected with lentiviral GFP or shPPA1 and collected at 0 days, 2 days, 6 days post induction. RNA was extracted according to the above method. Sequencing data was generated on an Illumina Solexa. Sequencing data QC was performed using fastqc and trimmomatic. Differential gene expression compared to undifferentiated (0 day) was assessed using three pipelines: Kallisto, followed by Sleuth; Star followed by Cutdiff; and star followed by HTseq and DESeq2. Differential gene expression was called significant if p-value < 0.05 for all three pipelines.

Western blot analysis

Total proteins of the tissues or cells were extracted by the RIPA buffer (Beyotime, China) containing protease inhibitor cocktail. The protein concentration was determined by the BCA protein assay. Lysates were subjected to Western blotting and proteins were detected by corresponding antibodies. The protein bands were imaged using the Tanon 5200 CL imaging analysis system. Antibodies against ACC (#3662), AP2 (#2120), FASN (#3189), p-IR (#3024 S), IR (#3025 S), p-AKT (#13038 S), AKT (#4691 S), C/EBPδ (#2318), CREB (#9197 S), p-CREB (#9198), CDK2(#2546) were obtained from Cell Signaling Technology. Antibodies against PPA1 (ab175233), UCP1 (ab10983), PGC1α (ab54481), SREBP1C (ab28481), C/EBPβ (ab15050), p27 KIP1(ab927411) were obtained from Abcam. Antibodies against PPARγ (sc-7273) were obtained from Santa Cruz Biotech. Antibodies against Tubulin (BS1482MH), GAPDH (MB001H) were obtained from Bioworld. The intensities of protein bands were quantified using the Image J software.

Co-immunoprecipitation (Co-IP)

For Co-IP assay, protein lysates were prepared from 3T3-L1 cells differentiated for 0, 12 and 24 h in a buffer containing 50 mM Tris-HCl (pH 7.5), 150 mM NaCl, 0.1% NP-40, and a mixture of protease inhibitors. Then, 500 mg of cell lysate were incubated with Protein A Magnetic beads and PPA1 antibody for 12 h at 4°C. On the next day, beads were washed three times with lysis buffer for 2 min and collected by magnetic attraction between each wash. The eluted protein was then subjected to western blot analysis.

Immunofluorescence and EdU staining

For the Immunofluorescence staining assay, 3T3-L1 cells were differentiated for 24 h and plated on coverslips. After adherence, cells were fixed for 15 min with 4% PFA in PBS, permeabilized in 0.2% Triton X-100 in PBS for 10 min and blocked using 5% BSA for 1 h at RT. Then, cells were stained with indicated primary antibodies followed by incubated with fluorescent-conjugated secondary antibodies. The nuclei were counterstained with DAPI (Sigma-Aldrich, #MBD0020). Images were captured using a confocal scanning fluorescence microscope (FV1200, Olympus, Japan).

For the EdU staining assay, 3T3-L1 preadipocytes were infected with lentiviral vector expressing control (GFP) or PPA1 knockdown shRNAs (shPPA1) and plated on coverslips. Cells were incubated with EdU (#C10310, RiboBio, China) for 2 h and then fixed in 4% PFA and incubated with glycine (2 mg/ml). Then cells were stained with Apollo solution for 30 min and the nuclei were counterstained with DAPI. Images were captured using a confocal microscope. Three random positions in each coverslip were photographed, and the fluorescence of EdU-positive cells was measured using ImageJ software.

Statistical analysis

All experiments were conducted three times unless otherwise specified in this study. Sample sizes were determined based on the amount of data required to give the statistical significance. No data were excluded from the study. Data are represented as the means ± S.E.M and the error bars represent the standard error of mean. Significant differences were assessed using a two-tailed Student's *t*-test or one-way *ANOVA* analysis. The P value < 0.05 was considered significant. Statistical analyses were performed in Microsoft Excel and GraphPad Prism (version 8.0).

DATA AVAILABILITY

The raw RNA-sequencing data reported in this paper have been deposited in the Figshare database (https://doi.org/10.6084/m9.figshare.25679760). All datasets analyzed in the study are available from the corresponding authors on reasonable request. Raw western blots are available in the Supplemental file.

REFERENCES

1. Hirsch J, Han PW. Cellularity of rat adipose tissue: effects of growth, starvation, and obesity. J Lipid Res. 1969;10:77–82.
2. Kloting N, Bluher M. Adipocyte dysfunction, inflammation and metabolic syndrome. Rev Endocr Metab Disord. 2014;15:277–87.
3. Sun K, Tordjman J, Clement K, Scherer PE. Fibrosis and adipose tissue dysfunction. Cell Metab. 2013;18:470–7.
4. Hardy OT, Perugini RA, Nicoloro SM, Gallagher-Dorval K, Puri V, Straubhaar J, et al. Body mass index-independent inflammation in omental adipose tissue associated with insulin resistance in morbid obesity. Surg Obes Relat Dis. 2011;7:60–7.
5. Kloting N, Fasshauer M, Dietrich A, Kovacs P, Schon MR, Kern M, et al. Insulin-sensitive obesity. Am J Physiol Endocrinol Metab. 2010;299:E506–15.
6. Vishvanath L, Gupta RK. Contribution of adipogenesis to healthy adipose tissue expansion in obesity. J Clin Invest. 2019;129:4022–31.
7. Ghaben AL, Scherer PE. Adipogenesis and metabolic health. Nat Rev Mol Cell Biol. 2019;20:242–58.
8. Quinn K, Chauhan S, Purcell SM. Lipodystrophies. In: StatPearls [Internet]. Treasure Island (FL): StatPearls Publishing; 2024.
9. Mann JP, Savage DB. What lipodystrophies teach us about the metabolic syndrome. J Clin Invest. 2019;129:4009–21.
10. Zammouri J, Vatier C, Capel E, Auclair M, Storey-London C, Bismuth E, et al. Molecular and Cellular Bases of Lipodystrophy Syndromes. Front Endocrinol (Lausanne). 2021;12:803189.
11. Mota de Sa P, Richard AJ, Hang H, Stephens JM. Transcriptional regulation of adipogenesis. Compr Physiol. 2017;7:635–74.
12. White U, Fitch MD, Beyl RA, Hellerstein MK, Ravussin E. Adipose depot-specific effects of 16 weeks of pioglitazone on in vivo adipogenesis in women with obesity: a randomised controlled trial. Diabetologia. 2021;64:159–67.
13. McLaughlin TM, Liu T, Yee G, Abbasi F, Lamendola C, Reaven GM, et al. Pioglitazone increases the proportion of small cells in human abdominal subcutaneous adipose tissue. Obes (Silver Spring). 2010;18:926–31.
14. Sarjeant K, Stephens JM. Adipogenesis. Cold Spring Harb Perspect Biol. 2012;4:a008417.
15. Lee JE, Ge K. Transcriptional and epigenetic regulation of PPARgamma expression during adipogenesis. Cell Biosci. 2014;4:29.
16. Cao Z, Umek RM, McKnight SL. Regulated expression of three C/EBP isoforms during adipose conversion of 3T3-L1 cells. Genes Dev. 1991;5:1538–52.
17. Yeh WC, Cao Z, Classon M, McKnight SL. Cascade regulation of terminal adipocyte differentiation by three members of the C/EBP family of leucine zipper proteins. Genes Dev. 1995;9:168–81.
18. Tanaka T, Yoshida N, Kishimoto T, Akira S. Defective adipocyte differentiation in mice lacking the C/EBPbeta and/or C/EBPdelta gene. EMBO J. 1997;16:7432–43.

19. Guo L, Huang JX, Liu Y, Li X, Zhou SR, Qian SW, et al. Transactivation of Atg4b by C/EBPbeta promotes autophagy to facilitate adipogenesis. Mol Cell Biol. 2013;33:3180–90.
20. Tang QQ, Otto TC, Lane MD. Mitotic clonal expansion: a synchronous process required for adipogenesis. Proc Natl Acad Sci USA. 2003;100:44–9.
21. Tezuka Y, Okada M, Tada Y, Yamauchi J, Nishigori H, Sanbe A. Regulation of neurite growth by inorganic pyrophosphatase 1 via JNK dephosphorylation. PLoS One. 2013;8:e61649.
22. Polewski MD, Johnson KA, Foster M, Millan JL, Terkeltaub R. Inorganic pyrophosphatase induces type I collagen in osteoblasts. Bone. 2010;46:81–90.
23. Luo D, Liu D, Shi W, Jiang H, Liu W, Zhang X, et al. PPA1 promotes NSCLC progression via a JNK- and TP53-dependent manner. Oncogenesis. 2019;8:53.
24. Mishra DR, Chaudhary S, Krishna BM, Mishra SK. Identification of critical elements for regulation of inorganic pyrophosphatase (PPA1) in MCF7 Breast Cancer Cells. PLoS One. 2015;10:e0124864.
25. Tomonaga T, Matsushita K, Yamaguchi S, Oh-Ishi M, Kodera Y, Maeda T, et al. Identification of altered protein expression and post-translational modifications in primary colorectal cancer by using agarose two-dimensional gel electrophoresis. Clin Cancer Res. 2004;10:2007–14.
26. Chen G, Gharib TG, Huang CC, Thomas DG, Shedden KA, Taylor JM, et al. Proteomic analysis of lung adenocarcinoma: identification of a highly expressed set of proteins in tumors. Clin Cancer Res. 2002;8:2298–305.
27. Yin Y, Wu Y, Zhang X, Zhu Y, Sun Y, Yu J, et al. PPA1 regulates systemic insulin sensitivity by maintaining adipocyte mitochondria function as a novel PPARgamma target gene. Diabetes. 2021;70:1278–91.
28. Stern JH, Rutkowski JM, Scherer PE. Adiponectin, leptin, and fatty acids in the maintenance of metabolic homeostasis through adipose tissue crosstalk. Cell Metab. 2016;23:770–84.
29. Cavalcanti-de-Albuquerque JP, Bober J, Zimmer MR, Dietrich MO. Regulation of substrate utilization and adiposity by Agrp neurons. Nat Commun. 2019;10:311.
30. Chhabra KH, Adams JM, Fagel B, Lam DD, Qi N, Rubinstein M, et al. Hypothalamic POMC deficiency improves glucose tolerance despite insulin resistance by increasing glycosuria. Diabetes. 2016;65:660–72.
31. Lahti R, Kolakowski LF Jr., Heinonen J, Vihinen M, Pohjanoksa K, Cooperman BS. Conservation of functional residues between yeast and E. coli inorganic pyrophosphatases. Biochim Biophys Acta. 1990;1038:338–45.
32. Vihinen M, Lundin M, Baltscheffsky H. Computer modeling of two inorganic pyrophosphatases. Biochem Biophys Res Commun. 1992;186:122–8.
33. Gustafson B, Hammarstedt A, Hedjazifar S, Smith U. Restricted adipogenesis in hypertrophic obesity: the role of WISP2, WNT, and BMP4. Diabetes. 2013;62:2997–3004.
34. Tchoukalova YD, Votruba SB, Tchkonia T, Giorgadze N, Kirkland JL, Jensen MD. Regional differences in cellular mechanisms of adipose tissue gain with overfeeding. Proc Natl Acad Sci USA. 2010;107:18226–31.
35. Cristancho AG, Lazar MA. Forming functional fat: a growing understanding of adipocyte differentiation. Nat Rev Mol Cell Biol. 2011;12:722–34.
36. Farmer SR. Transcriptional control of adipocyte formation. Cell Metab. 2006;4:263–73.
37. Hattori T, Ohoka N, Inoue Y, Hayashi H, Onozaki K. C/EBP family transcription factors are degraded by the proteasome but stabilized by forming dimer. Oncogene. 2003;22:1273–80.
38. Li H, Xiao N, Li Z, Wang Q. Expression of Inorganic Pyrophosphatase (PPA1) Correlates with Poor Prognosis of Epithelial Ovarian Cancer. Tohoku J Exp Med. 2017;241:165–73.
39. Niu H, Zhou W, Xu Y, Yin Z, Shen W, Ye Z, et al. Silencing PPA1 inhibits human epithelial ovarian cancer metastasis by suppressing the Wnt/beta-catenin signaling pathway. Oncotarget. 2017;8:76266–78.
40. Siersbaek R, Nielsen R, Mandrup S. Transcriptional networks and chromatin remodeling controlling adipogenesis. Trends Endocrinol Metab. 2012;23:56–64.
41. Lim GE, Albrecht T, Piske M, Sarai K, Lee JTC, Ramshaw HS, et al. 14-3-3zeta coordinates adipogenesis of visceral fat. Nat Commun. 2015;6:7671.
42. Tang QQ, Otto TC, Lane MD. CCAAT/enhancer-binding protein beta is required for mitotic clonal expansion during adipogenesis. Proc Natl Acad Sci USA. 2003;100:850–5.
43. Audano M, Pedretti S, Caruso D, Crestani M, De Fabiani E, Mitro N. Regulatory mechanisms of the early phase of white adipocyte differentiation: an overview. Cell Mol Life Sci. 2022;79:139.
44. Tang QQ, Lane MD. Adipogenesis: from stem cell to adipocyte. Annu Rev Biochem. 2012;81:715–36.
45. Guo L, Li X, Tang QQ. Transcriptional regulation of adipocyte differentiation: a central role for CCAAT/enhancer-binding protein (C/EBP) beta. J Biol Chem. 2015;290:755–61.
46. Liu Y, Zhang YD, Guo L, Huang HY, Zhu H, Huang JX, et al. Protein inhibitor of activated STAT 1 (PIAS1) is identified as the SUMO E3 ligase of CCAAT/enhancer-binding protein beta (C/EBPbeta) during adipogenesis. Mol Cell Biol. 2013;33:4606–17.
47. Chung SS, Ahn BY, Kim M, Choi HH, Park HS, Kang S, et al. Control of adipogenesis by the SUMO-specific protease SENP2. Mol Cell Biol. 2010;30:2135–46.
48. Ramji DP, Foka P. CCAAT/enhancer-binding proteins: structure, function and regulation. Biochem J. 2002;365:561–75.
49. Lechner S, Mitterberger MC, Mattesich M, Zwerschke W. Role of C/EBPbeta-LAP and C/EBPbeta-LIP in early adipogenic differentiation of human white adipose-derived progenitors and at later stages in immature adipocytes. Differentiation. 2013;85:20–31.
50. Wang P, Zhou Y, Mei Q, Zhao J, Huang L, Fu Q. PPA1 regulates tumor malignant potential and clinical outcome of colon adenocarcinoma through JNK pathways. Oncotarget. 2017;8:58611–24.
51. Tchoukalova YD, Harteneck DA, Karwoski RA, Tarara J, Jensen MD. A quick, reliable, and automated method for fat cell sizing. J Lipid Res. 2003;44:1795–801.
52. Bahrami-Nejad Z, Zhao ML, Tholen S, Hunerdosse D, Tkach KE, van Schie S, et al. A transcriptional circuit filters oscillating circadian hormonal inputs to regulate fat cell differentiation. Cell Metab. 2018;27:854–68.e8.
53. Shamsi F, Tseng YH. Protocols for generation of immortalized human brown and white preadipocyte cell lines. Methods Mol Biol. 2017;1566:77–85.
54. Heinonen JK, Lahti RJ. A new and convenient colorimetric determination of inorganic orthophosphate and its application to the assay of inorganic pyrophosphatase. Anal Biochem. 1981;113:313–7.

ACKNOWLEDGEMENTS

We thank all the lab members for insightful discussion during this study.

AUTHOR CONTRIBUTIONS

YY and HYL conceived the project and wrote the manuscript. YYW and YS designed and performed most experiments. YQS performed in vivo studies and analyzed the data. YH and JTW performed in vitro experiments. XH contributed to the discussion and critically reviewed and edited the manuscript. All authors revised and approved the final version of the manuscript. XH is the guarantor of this work and, as such, had full access to all the data in the study and takes responsibility for the integrity of the data and the accuracy of the data analysis.

FUNDING

This work was supported by National Key R&D Program of China (2022YFA0806102), National Natural Science Foundation of China (82270874, 82370855, 81970709).

COMPETING INTERESTS

The authors declare no competing interests.

ETHICS

All animal experiments were approved and complied with the guidelines of the Institutional Animal Care and Use Committee of the Nanjing Medical University, China (Permit Number: IACUC-NJMU 14030178). Human specimens were supplied by the Southeast University Affiliated Zhongda Hospital and written informed consent was obtained from the patients (Permit number: 2020ZDSYLL144-P01 by the Independent Ethics Committee of Southeast University Affiliated Zhongda Hospital).

ADDITIONAL INFORMATION

Supplementary information The online version contains supplementary material available at https://doi.org/10.1038/s41418-024-01309-2.

Correspondence and requests for materials should be addressed to Haiyan Lin, Ye Yin or Xiao Han.